ACS APPLIED MATERIALS & INTERFACES

Research Article

www.acsami.org

Scalable Low-Cost Fabrication of Disposable Paper Sensors for DNA Detection

Ram P. Gandhiraman,[†] Dennis Nordlund,[‡] Vivek Jayan,[†] M. Meyyappan,*[,†] and Jessica E. Koehne[†]

[†]NASA Ames Research Center, Moffett Field, California 94035, United States

[‡]Stanford Synchrotron Radiation Lightsource, SLAC National Accelerator Laboratory, Menlo Park, California 94025, United States

Supporting Information

ABSTRACT: Controlled integration of features that enhance the analytical performance of a sensor chip is a challenging task in the development of paper sensors. A critical issue in the fabrication of low-cost biosensor chips is the activation of the device surface in a reliable and controllable manner compatible with large-scale production. Here, we report stable, well-adherent, and repeatable site-selective deposition of bioreactive amine functionalities and biorepellant polyethylene glycol-like (PEG) functionalities on paper sensors by aerosol-assisted, atmospheric-pressure, plasma-enhanced chemical vapor deposition. This approach requires only 20 s of deposition time, compared to previous reports on cellulose functionalization, which takes hours. A detailed analysis of the near-edge X-ray absorption fine structure (NEXAFS) and its sensitivity to the local electronic structure of the carbon and nitrogen functionalities. σ^*, π^*, and Rydberg transitions in C and N K-edges are presented. Application of the plasma-processed paper sensors in DNA detection is also demonstrated.

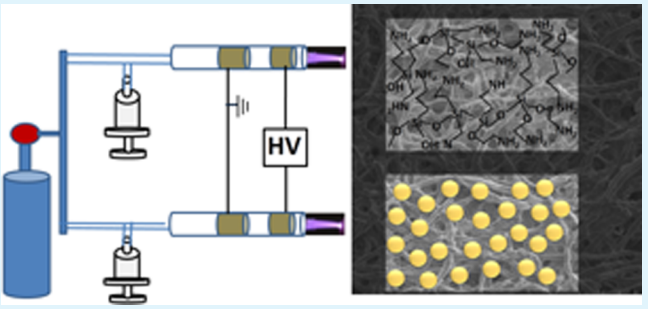

KEYWORDS: *paper sensors, DNA detection, X-ray absorption, NEXAFS, cellulose functionalization*

INTRODUCTION

Paper-based sensors are the most recent development in low-cost point-of-care diagnostics.[1] The need for deoxyribonucleic acid (DNA) detection is growing rapidly, because of its application in a wide range of fields including DNA diagnostics, forensic detection, and biothreat detection.[2] DNA detection, using cellulose paper as the substrate, has recently gained much attention.[3−6] Functionalization of cellulose fibers and incorporation of signal amplification elements are key aspects of paper sensor fabrication. Surface functionalization of bioreactive organic chemical groups is essential for covalently immobilizing the bioreceptor molecules to the sensor surface, and biorepellent organic functionalities are essential to reduce the nonspecific binding. Reduced nonspecific binding is critical to prevent analyte loss through nonspecific binding in the flow channels before it arrives at the detection site and also to prevent binding of nonanalyte constituents at the detection site. Cellulose fiber functionalization for DNA detection is typically performed via liquid-phase processing.[5,6] Su et al. demonstrated covalent binding of aptamers,[7] and Sharma et al. used functionalization with a photoreactive compound, followed by ultraviolet (UV) activation.[8] Aied et al. demonstrated nanogram-range detection of nucleic acids on cellulose paper using a surface-grown cationic polymer.[9,10] The strategies used thus far in the literature require multiple processing steps, preprocessing prior to the actual functionalization and a time-consuming drying step, all together requiring two to several hours. To the best of our knowledge, industrially friendly and high-throughput gas-phase functionalization of cellulose for any application has not been reported. In this work, we demonstrate a low-cost, rapid functionalization process that requires only 20 s, which can be scaled easily for parallel as well as batch high-throughput processing.

Amine functionalization is a well-known surface chemical modification for covalent immobilization of bioreceptor molecules. Poly(ethylene glycol) (PEG)-based coatings are widely used for reducing nonspecific binding. Low-pressure, vacuum-chamber-based, plasma deposition of bioreactive amine and biorepellant PEG has been demonstrated by several groups.[11,12] The drawback with using low-pressure plasma deposition in fabricating paper sensors is that the entire sensor surface will be coated and site-selective deposition is not possible without a vacuum seal mask, which increases both the complexity and the production cost. The development of atmospheric-pressure microplasmas has revolutionized the plasma processing technology in recent years.[13] In the present work, we have deposited the bioreactive and biofouling coatings site selectively on cellulose fibers, using a maskless, atmospheric-pressure plasma jet. The bioreactive amine functional group was deposited using amino propyl triethoxysilane (APTES), and the biorepellant PEG was deposited using diethylene glycol dimethyl ether.

Received: October 7, 2014
Accepted: November 25, 2014
Published: November 25, 2014

Metal nanostructures in a dielectric medium have been widely used as signal transduction element; examples include label-free localized surface plasmon resonance-based detection, because of its sensitivity to local changes in dielectric environment, and also as a signal amplification element in fluorescence-based detection through metal-enhanced fluorescence.[14] Incorporation of gold nanoparticles in the sensor chip offers several advantages, such as signal amplification and/or signal transduction. Several groups have demonstrated the application of gold-nanorod-incorporated plasmonic paper sensor for label-free diagnostics.[14,15] Gold nanostructures have also been used in fluorescence-based labeled detection for signal amplification through surface plasmon-coupled emission.[16] Here, we demonstrate incorporation of metal nanostructures on paper substrates using a high-throughput aerosol-assisted atmospheric-pressure plasma process. Gold nanoparticles were deposited by aerosolizing the gold colloid and introducing the aerosol into the plasma jet.[17]

Development of multifunctional paper platforms combining the above functionalities would typically require several sequential processing steps using different tools for each processing step; no single tool is available to perform most of the functions required in the fabrication of the sensor. In this work, we report site-selective plasma functionalization of bioreactive and biorepellant groups on cellulose fibers and also incorporate metal nanoparticles: all are steps using just one single tool. Since the immobilization efficiency and the device performance are dependent on the chemical constituent and the surface properties, X-ray photoelectron spectroscopy (XPS) and X-ray absorption spectroscopy (XAS) techniques were used for a detailed surface chemical analysis. In particular, we paid special attention to the application of near-edge X-ray absorption fine structure (NEXAFS) to elucidate the chemical species and electronic structure and to unambiguously identify the level of unsaturation in the plasma-polymerized films.

EXPERIMENTAL SECTION

Paper Sensor Fabrication. Our plasma system consists of a glass tube with an outer diameter of 5 mm, and two copper tapes separated by 20 mm are wound over the glass tube to form concentric outer electrodes (see Figure 1, presented later in this work, for a schematic of the setup). Helium is used as a plasma gas source, and a high voltage that is applied between the electrodes causes the gas to break down within the central core of the glass capillary, generating plasma at atmospheric pressure. Nanostructure colloids and the organic precursors are placed in a glass container with an inlet and outlet for carrier gas and are seated on an ultrasonic nebulizer. There is also an additional gas input line to facilitate ignition, as well as to focus the spot size. Helium is also flown into the nebulizer via a gas input line. The aerosol is then carried into the plasma stream by the carrier gas and deposited onto the substrate. The spot size can be altered by altering the print head nozzle diameter. Bioreactive amine functional group is deposited using APTES and the biorepellant PEG is deposited using diethylene glycol dimethyl ether. Both precursors are individually aerosolised to the plasma jet and directed toward the surface to be coated.

Whatman cellulose filter paper samples were used here for functionalization and DNA hybridization. Both unpatterned filter paper and a wax patterned filter paper were functionalized. Wax patterned paper containing hydrophobic and hydrophilic regions were prepared based on information from previous reports.[18,19] Amine and PEG-like functionalization was performed on the exposed paper region.

Characterization. Fourier transform infrared (FTIR) spectroscopic measurements were carried out using a Perkin–Elmer Mode Spectrum GX FTIR system. Single-side polished silicon wafers were used as substrates for the transmission mode measurement. An untreated silicon substrate was used as a background substrate, and all measurements were an average of 250 scans. Scanning electron microscopy (SEM) imaging was performed using an SEM microscope system (Model S4800, Hitachi, Pleasanton, CA). As-deposited paper samples were used for imaging without any additional charge neutralizing metal coating.

The C 1s and N 1s NEXAFS and XPS measurements were performed on beamline 8-2 (bending magnet end station, spherical grating monochromator) at the Stanford Synchrotron Radiation Lightsource (SSRL).[20] A gold grid in the beam path upstream of the chamber was used for normalization of the incoming flux. The samples were mounted on an aluminum stick with carbon tape and all the measurements were done under UHV conditions ($<1 \times 10^{-8}$ Torr) in a generic XAS/XPS chamber. The energy was calibrated at the carbon dip (284.7 eV) and the second order Ni 2p edge of NiO, mounted on a reference sample upstream of the chamber. The drain current from the isolated aluminum stick was used for total electron yield (TEY). All NEXAFS spectra were divided by the incoming flux measured by the gold grid, and normalized 20–30 eV above the ionization potential. A double-pass cylindrical mirror analyzer was used for the photoelectron spectroscopy measurements. The beamline slits and the pass energy of the analyzer were set for a total energy resolution below 0.7 eV for the XPS measurements and below 0.3 eV for the NEXAFS measurements. All measurements were performed at the magic angle (~55° incidence), and the spectrometer detected electrons emitted along the e-vector of the incoming radiation (90°, with respect to the incoming light in the horizontal plane).

Bioassay. DNA hybridization assays were carried out on plasma-coated cellulose acetate filter paper substrates. Three samples were used: amine-functionalized paper, gold-nanoparticle-coated paper, and untreated paper. For the DNA hybridization, the ssDNA containing amine functionalities in one end and Cy3 fluorophore on another end was used as the primary ligand, and the complementary DNA containing Cy5 fluorophore was used to detect the DNA hybridization. The oligos were purchased from Eurofins. The sequence for the probe ssDNA is 5′-Cy3[SP-3] AGAGAACCTGGG-$[TTT]_4$[SP-3][AmC7-Q]-3′, and the sequence for the target DNA is 5′-[Cy5]AAAAAAA···ACCCAGGTTCTCT-3′. For covalent immobilization of the amine-terminated oligos to amine-functionalized paper, a 2.5% glutaraldehyde cross-linker was used. Further DNA hybridization was carried out after dropcasting the complementary DNA. The probe concentration was 10 μM, and the target concentration was varied from 10 μM down to 10 nM. On the gold-nanoparticle-containing paper, the binding of amine-terminated probe oligos is through the affinity between gold–amine functionalities. The complementary DNA was dropcast directly onto the amine-functionalized paper and PEG-functionalized paper to study the nonspecific binding, and an untreated paper was used as control. An Affymetrix 428 array fluorescence scanner with Jaguar software (version 2.0) was used for fluorescence measurement (at a gain setting of 30). Fluorescence measure-

ments were carried out both after immobilization of the ligand oligos and DNA hybridization. The fluorescence intensity was calculated using the ImageJ software. The probe DNA with Cy3 was immobilized without using any cross-linkers to study gold-functionalized paper and the fluorescence imaging was performed in a Zeiss fluorescence microscope. Absorption and emission of the Cy3 fluorophore in primary ssDNA are at 550 and 570 nm. Absorption and emission of the Cy5 fluorophore in target DNA are observed at 649 and 670 nm.

RESULTS AND DISCUSSION

The schematic of the atmospheric plasma deposition system is shown in Figure 1a, and the photograph of the plasma

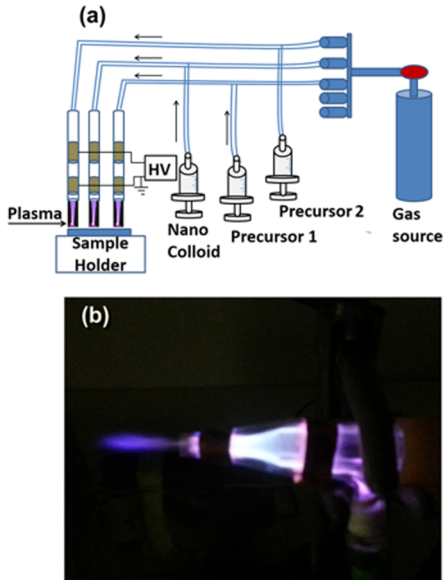

Figure 1. (a) Schematic of the atmospheric-pressure plasma jet system and (b) photograph of the plasma double-jet system.

discharge is shown in Figure 1b. In the aerosol-assisted plasma deposition process, an aerosol carrying at least one of the desired substances for deposition is introduced into a cold plasma jet operating at atmospheric pressure. The process uses a combination of low-temperature atmospheric-pressure plasma and the aerosol containing the material to be deposited. A plasma-polymerized film is formed when the aerosolized precursor material interacts with the plasma. The role of the atmospheric-pressure plasma is to activate the material present in the aerosol for deposition on the surface and to enhance the adhesion of the material on the surface; in addition, the plasma can facilitate nonaggregated deposition in the case of metal nanostructure/microstructure formation and plasma polymerization in the case of organic coating deposition through the formation of reactive radicals and ions as the aerosol enters the plasma jet. Helium is used as the primary gas source[21] for igniting and sustaining the plasma.

Surface amination of polymer substrates by plasma-enhanced chemical vapor deposition (PECVD) is routinely carried out using allylamine, ammonia, and nitrogen/hydrogen gases.[22,23] In low-pressure PECVD, APTES has an advantage over alkyl amine in determining the extent of amination and adhesion strength to surfaces upon rigorous washing.[12] The role of siloxane in anchoring to the plastic and metal surfaces for further plasma functionalization and cross-linking has been established previously.[24,25] We carried out the amine functionalization using APTES as the precursor material, since the adhesion of the functionalized coating to the cellulose fibers is critical for repeatable and reproducible bioassay performance. The schematic for binding of APTES to cellulose is shown in Figure 1c. The deposition time was fixed at 20 s, and no systematic variation was performed to study the effect of deposition time on surface functionalization and DNA hybridization. The objective here is to reduce the deposition time as much as possible from current practice in the literature, which ranges in hours. There was significant binding, even within 20 s; hence, longer durations were not attempted. The deposition rate generally varies from substrate to substrate. The measurement of film thickness on cellulose is challenging and, hence, has not been undertaken. However, the surface functionalization of paper sensors is confirmed here via detailed X-ray spectroscopic analysis of untreated and plasma-treated cellulose.

Figure 2 shows two types of cellulose paper samples used for functionalization and DNA hybridization. Figure 2a shows the paper patterned using wax printing. Amine and PEG-like functionalization were performed on the exposed paper region.

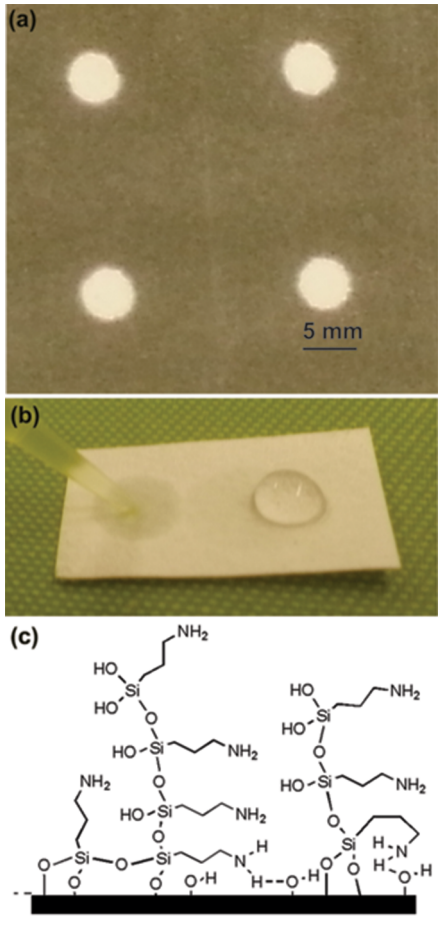

Figure 2. (a) Photograph of wax-coated paper. (b) Photograph of cellulose paper whose right half is coated with amine functionality and the left half is untreated. In the untreated region, the water droplet spreads due to high surface tension. In the amine-functionalized region, the water droplet maintains a higher contact angle. (c) Schematic of randomly oriented plasma polymerized film bonded through the hydroxyl group of the cellulose fiber.

Figure 2b shows the paper whose right half is coated with amine functionality and the left half left untreated. A water droplet was placed on both regions and an optical photograph was taken. The water spreads immediately in the untreated region. The amine-functionalized region shows hydrophobic behavior and the water droplet forms a higher contact angle with the surface (Figure 2b, right half); the droplet then slowly wicks through the surroundings as time passes.

A stable amino functionalization of cellulose can be formed through the siloxane functionality in the amino silane precursor. The plasma containing a silane/siloxane precursor is known to create highly reactive radicals and ions through fragmentation of the precursor.[26] We hypothesize that the interaction of highly reactive Si- and SiO-based radicals with OH and C−O functionalities in the cellulose resulted in surface amination of the paper fibers. Bierbaum et al., in their angle-dependent NEXAFS measurement on self-assembled amino silane monolayers, observed that the films have no defined orientation of the molecules.[27] Based on this, we assume that our plasma polymer layers are also randomly polymerized on the surface and do not exhibit any defined orientational order. Figure 2b shows a hypothesized structure of the randomly oriented functionalized molecules.

Characterization Results. Figure 3a displays the FTIR spectrum of the amine-functionalized layer. The presence of the amine group can be characterized by asymmetric and symmetric N−H stretching bands between 3380 cm^{-1} and 3350 cm^{-1} and between 3310 cm^{-1} and 3280 cm^{-1} and N−H deformation between 1650 cm^{-1} and 1580 cm^{-1}.[28] The peak at 1630 corresponds to N−H bending vibration of free amine and the peak at 1585 cm^{-1} corresponds to N−H bending vibration of amine group, which is hydrogen-bonded either to hydroxyl groups in silanol in the bulk of the film or to cellulose at the interface.[29] The region between 3000 cm^{-1} and 3500 cm^{-1} displays a broad, asymmetric peak shape that indicates multiple components. The OH stretching mode of the associated silanol group is ∼3350 cm^{-1}.[30] The multiple bands between 2883 cm^{-1} and 2976 cm^{-1} correspond to the stretching vibrations of $O-CH_x$ groups and CH_x groups deposited from the ethoxy component of the precursor. We also associate 2970 cm^{-1} with CH_3 asymmetric stretching, 2926 cm^{-1} with CH_2 asymmetric stretching, 2886 cm^{-1} with CH_2 symmetric stretching, and 1390 cm^{-1} with CH_3 symmetric deformation.[31] The intense, multiple peaks at 1078, 1112, and 1182 cm^{-1} correspond to Si−O−Si vibration and Si−O−C that are present both in the bulk of the coating and at the cellulose interface.[32] The IR absorption bands of amine and hydrocarbon-related functionalities are similar to that of the alkyl amine functionalities, except for the additional siloxane peaks arising from the silane precursor.[33]

The C 1s core-level photoemission spectra of the untreated paper sample and amine-functionalized paper are presented in Figure 3b. Both the spectra show very clear and distinct carbon bonding environments. The untreated paper shows three photoemission peaks centered at 284.3, 286.8, and 288.5 eV, attributed to unsaturated carbon, C−O, and O−C−O bonding, respectively. For the amine-functionalized paper samples, we observe photoemission peaks at 285.2 eV (C−C bond), 287.2 eV (C═N bonding in imine), 288.2 eV (C═O in amide), and a shoulder at 286.2 eV (C−N).[34,35] The photoemission spectra corresponding to various carbon bonding environments exhibit behavior similar to that of low-pressure plasma-polymerized amine functionalization.[12,36] The presence of oxygen in the amino silane precursor could have contributed to the formation of amide bonds. The confirmation of C−N bonding environment that corresponds to primary amine is essential as the primary amine molecules are used for covalent immobilization of the bioreceptor molecules to the paper sensor.

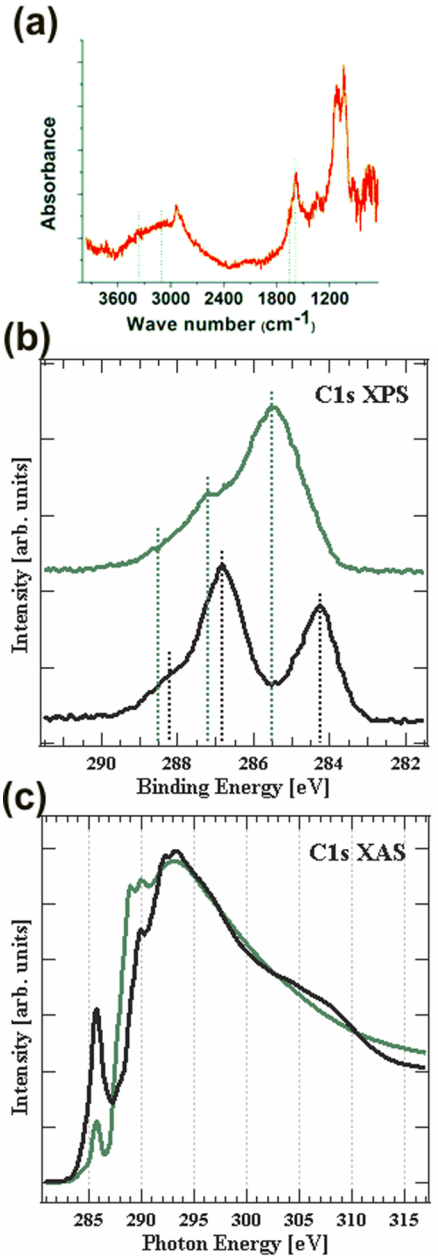

Figure 3. (a) FTIR spectrum of amine-functionalized coating. (b) C 1s core-level photoemission spectroscopy of untreated paper (black trace) and amine-functionalized cellulose (green trace). (c) C XAS of untreated paper (black trace) and aminated paper (green trace).

XAS (NEXAFS) was used to probe the local bonding environments. Apart from its elemental specificity, XAS is particularly sensitive to the local electronic structure, including angular anisotropy in molecular orientation, bond length, oxidation state, and symmetry, as well as spin.[37,38] When tuning an X-ray source (synchrotron) to match a core-level ionization potential, absorption of a photon can transition a core-level electron into unoccupied bound or continuum states. In particular, before the ionization potential, excitation to low-lying unoccupied molecular orbitals occurs, which are typically

π^* antibonding orbitals and mixed Rydberg/valence states. Transition to σ^* antibonding orbitals is seen above the ionization edge threshold at higher photon energies. XAS displays similar element specificity and local character as XPS (participation of core-hole), but with increased sensitivity to chemical environment through the unoccupied states.

Figure 3c shows the C 1s XAS spectrum of untreated paper and amine-functionalized paper taken at 54° relative to the surface, showing the unoccupied π^* and σ^* bands at 284−286 eV and 289−311 eV, respectively.[39,40] For untreated paper, an intense peak at 285.9 eV and a slight shoulder at 284.8 eV are observed in the π^* region, whereas the σ^* region displays a broad asymmetric peak centered at ∼309 eV and a broad shoulder at 304 eV. Following published works on unsaturated alcohols and carboxylic acids[40,41]—in particular, unsaturated propargyl alcohol,[41] propiolic acid,[40] and ethyne[42]—we associate C≡C bonds with the 285.9 eV (π^*) and 309 eV (σ^*) resonances, and we associate C═C bonds with the 284.8 eV (π^*) and 304 eV (σ^*) resonances. The resonance at 293.5 eV is attributed to σ^* transition of single bonded oxygen, based on Outka et al.[41] and Sette et al.[42] as hydroxyl groups form a major component of the cellulose network.

The C 1s NEXAFS spectra of amino-functionalized paper exhibit four intense peaks and a shoulder. We note the absence of σ^* transitions at 304 and 309 eV and the reduction of intensity near 285 eV, demonstrating that the majority of unsaturated C bonds have changed their chemical environment through amine functionalization. The nitrogen functionalization can be observed at 286 eV (assigned to C═N π^* transition) and above 289 eV (assigned to C−N σ^*).[43,44] This assignment is in agreement with the transition from unsaturated carbon to CN_x in XPS. The shoulder around 287.8 eV corresponds to carbonyl π^*C═O of $CONH_2$, based on the trends in carbonyl core (C═O) π^* transitions, as a function of electronegativity of the chemical environment, as reported by Urquhart and Ade.[45] An intense peak at 289.2 eV, which is clearly present in the aminated surface and absent in the cellulose sample, is assigned to σ^* CNH transition, and the broad shoulder at 299.2 is assigned to 1s to σ^* C−N of carbon in −CONH.[39] The broad nature of the transition to σ^* symmetry is due to the fact that excitation is close to continuum. Sharp π^* transitions and the broad σ^* transition are mainly due to the lifetime broadening, i.e., the lifetime of the final excited state.[37]

Solomon et al.,[46] in their solid-state C 1s NEXAFS study of carbohydrates, amino sugars, and aromatic alcohols, assigned the peaks between 289.3 eV and 289.5 eV to C 1s−3p/sigma*C−H Rydberg mixed-valence transitions and reasoned that such transitions are earlier reported for primary alcohols and hydroxylated aliphatic carbon in the same region.[47,48] Kaznacheyev et al.[49] in their NEXAFS study of amino acids reported the absence of Rydberg transition and also assigned the peak at 289.4 eV to σ^* CNH transition. Based on this and an investigation of the literature on Rydberg transitions (see the Supporting Information), we assign the strong high intense peak at 289.2 eV in amine-functionalized paper to σ^* CNH transition and also include the possibility of overlapping with C 1s−3p/sigma*C−H Rydberg mixed valence transitions. For both the untreated and treated paper samples, two strong peaks at ∼290.1 and 292.5 eV are assigned to C−H resonance and C−C σ^* transitions.[40,41,50] The shoulder peak at 288.2 eV in cellulose probably corresponds to excitations into orbitals of dominantly Rydberg character.[51]

The peak at 284.8 eV could possibly be due to C−H bond breakage by the X-ray beam and the formation of C═C bonds. The beam damage of organic molecules and formation of C═C unsaturation has been reported;[33,52]for example, Graf et al. observed the formation of C═C and C═N(imine) and C≡N(nitrile) groups in liquid-phase-deposited amino silane due to beam damage.[43] However, the intensity of the 285.9 eV peak in cellulose is rather high and it is highly unlikely to be solely caused by beam damage, in particular, given the limited X-ray intensity used in our experiment. The cellulose paper substrate was purchased from Sigma−Aldrich and used without additional treatment. Since no data sheets were provided on the exact composition or processing steps, we assume that unsaturated hydrocarbons are present in the cellulose paper due to the manufacturing process. Further studies with well-defined cellulose paper are planned for the future.

The N 1s core-level photo emission (XPS) spectra in Figure 4a exhibits a double peak: one centered at ∼399.9 eV and another at ∼400.8 eV, corresponding to the binding energy levels of aliphatic amine groups, which is in close agreement with self-assembled monolayer of amino silane films.[27] The 399.9 eV corresponds to free amine and 400.9 eV corresponds to amine groups hydrogen-bonded to neighboring groups in

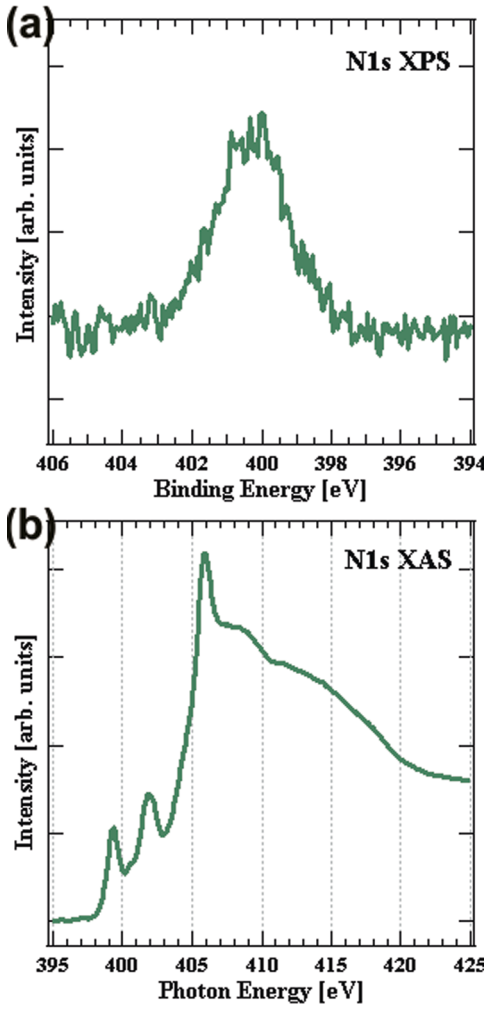

Figure 4. (a) N 1s core-level photo electron spectroscopy of amine-functionalized paper; (b) N 1s X-ray absorption spectroscopy of amine-functionalized paper.

the film. These peak attributions are made based on the literature on XPS analysis of aminosilane coatings.[53−55] A peak at 940 cm^{-1} in the FTIR spectra shows the presence of silanol (Si−OH groups) in the film. Since it is a plasma-polymerized film deposited using amino silane, the silanol group could be present throughout the film and oriented randomly. Hydrogen bonding between the free amine group in the film and the neighboring silanols groups results in increased binding energy and, hence, a peak at higher energy (400.8 eV, compared to 399.9 eV for free amines).[53] A shoulder peak observed at ∼399 eV can probably be associated with an imine group, but, as reported by Harder et al.,[53] imine and free amine are expected to overlap in XPS.

The N K-edge NEXAFS spectra Figure 4b shows distinct features with three sharp absorption peaks at 399.3, 401.9, and 405.9 eV. Small shoulders appear at 400.6 and 404.8 eV and two broad peaks are found at ∼408.9 and 411 eV. As Stohr et al.[50,56,57] have shown, there is a near linear relationship between σ^* transition energies and bond lengths to atoms adjacent to the core excited atom, the so-called "bond-length with a ruler"; for example, the shorter length of the partially conjugated amide C−N bond gives rise to a shift to higher transition energy for σ^* CONH, compared to σ^* C−NH_2.[58] This can be used to associate the N 1s → σ^* resonances in the NEXAFS spectrum with the main functional groups, i.e., free amine (405.9 eV, C−NH_2) hydrogen-bonded amine (408.9 eV, C−NH), and amide (411 eV, CONH). These peak assignments are in agreement with NEXAFS studies of peptides and amides by Ishii and Hitchcock,[59] Gordon et al.,[58] and Hitchcock et al.[60] Shard et al.[61] assigned a broad peak at ∼411 eV to C═N transitions that overlap with amide (CONH). The shoulder centered at ∼404.8 eV probably corresponds to mild oxidation of nitrogen and the formation of nitro compounds.[62]

The intense peaks in lower energy level at 399.3 and 401.9 eV are assigned to CN π^* and CONH π^* transitions, respectively. These peak assignments are in agreement with the observations of Hitchcock et al. on N 1s edge NEXAFS studies of polyacrylonitrile polymers and peptides,[63] Gordon et al. on solid-state peptides,[58] and Zhu et al.[64] on aliphatic amines. Shard et al.[61] have assigned 401.3 eV peak to σ^* N−H resonance. (See the Supporting Information.)

In summary, based on the spectroscopy characterization, the presence of free amine, hydrogen-bonded amine, and amide is evident from XPS C 1s core-level photoemission spectrum and FTIR spectrum, in agreement with the C 1s NEXAFS analysis. The C 1s and N 1s NEXAFS spectra show the presence of sp_2 hybridized states, confirming the formation of doubly bonded C, N, and O in the aminated surface. This is probably caused by electron-, ion-, and/or free-radical-initiated fragmentation and cross-linking of the plasma-polymerized films. We find that the bonding environment is more unambiguously probed in NEXAFS than the XPS. The assigned C 1s and N 1s NEXAFS resonances are summarized in Tables 1 and 2.

DNA Hybridization Results. DNA hybridization was carried out on a cellulose paper sensor surface treated with amine functionalization. The amine-functionalized ssDNA (probe) is covalently immobilized on the amine-functionalized paper sensor using glutaraldehyde cross-linker. The immobilized ssDNA is then imaged using a fluorescence scanner. The complementary DNA is then dropcast and the DNA hybridization is allowed to proceed, and the samples are scanned using the fluorescence scanner to detect the Cy5 fluorescence. As seen in Figure 5, the amine-functionalized paper shows a very large fluorescence intensity with saturation level. Varying the concentration level of the target DNA from 10 μM down to 10 nM results in a decrease in fluorescence intensity (Figure 5a). Three different surfaces were considered to test the nonspecific binding: amine-functionalized paper, PEG-like functionalized paper, and untreated paper. The PEG-like functionalization exhibits the least nonspecific binding followed by the untreated paper, with the amine-functionalized paper finishing last (see Figure 5b). Several mechanisms had been proposed for the protein-resistant nature of the PEG-like films including steric stabilization, water barrier theory, thermodynamic approach, etc.[65,66]Protein interaction on PEG-like coatings has been discussed by Menzies et al.[65] The details on such mechanisms are beyond the scope of this work, but the plasma processing parameters must be tailored here to deposit high-quality, biorepellant, PEG-like coatings.

Table 1. C K-Edge NEXAFS Peak Positions and Attribution

cellulose	aminated cellulose	assignments
284.8 eV (shoulder)	284.8 eV (shoulder)	probably beam damage
		π^* C═C
285.9 eV (intense)		π^* C≡C
		(σ^* at 308)
	286 eV (intense)	π^* C═N
	287.8 eV shoulder	carbonyl C═O π^*
288.1 eV (shoulder)		probably corresponds to excitations into orbitals of dominantly C−H* resonance
	289.1 eV (intense)	σ^* CNH
	clearly not present in cellulose	σ^* CH and 1s−3p Rydberg (Rydberg mixed-valence transitions)
290.1 eV (intense)	290.2 eV (intense)	1s to σ^* C−H/3p
		σ^* C−H
292.5 eV intense	292.5 eV broad	C−H resonance
		alkanes, C−C σ^*
293.5 eV (intense)	293.4 eV (intense broad)	C−O σ^*
297 eV (broad)		σ^* O−C−O
	299 eV (broad)	1s to σ^* C−N of carbon in −CONH
304 eV broad		σ^* C═C
309 eV (broad)		σ^* C≡C
	308 eV	C═O σ^*

Table 2. N K-Edge NEXAFS Peak Positions and Attribution

peak position	assignment
399.3 eV (intense)	π^* N═C
400.6 eV (minor)	π^* C≡N/σ^* N−H
401.9 eV (intense)	π^* CONH
404.8 eV (shoulder)	nitro compound
405.9 eV (intense)	σ^* N−C
	σ^* NH2
408.9 eV (shoulder)	σ^* NH
411 eV broad	σ^* N═C
	σ^* CONH

dx.doi.org/10.1021/am5069003 | ACS Appl. Mater. Interfaces 2014, 6, 22751−22760

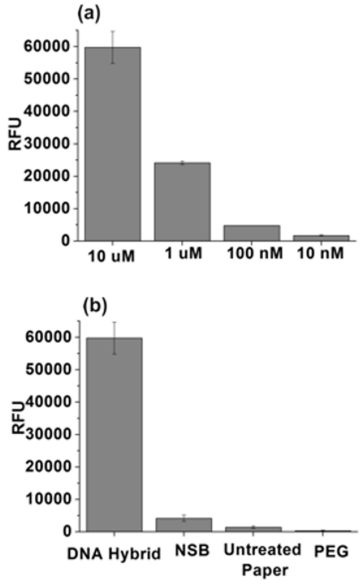

Figure 5. (a) ssDNA with 10 μM concentration bound to aminated paper using glutaraldehyde cross-linker. Complementary DNA containing Cy5 fluorophore with varying concentrations (from 10 μM down to 10 nM) is dropcast for hybridization. (b) DNA hybridization on aminated paper showing specific binding and nonspecific binding (NSB) of the target DNA to the aminated surface, the untreated paper, and the PEG-coated paper.

A comparatively higher nonspecific binding on amine-functionalized paper than on the untreated paper is likely due to the positively charged nature of the aminated surface. The DNA backbone, being negatively charged, could be expected to show higher nonspecific binding to the positively charged aminated surface than the untreated surface. However, the fluorescence intensity corresponding to specific binding on the amine-functionalized surface is significantly higher than the nonspecific binding, which demonstrates the usefulness of plasma functionalization of the paper sensors for DNA detection.

Metal nanostructures could enhance the analytical performance either through surface plasmon-enhanced coupling in fluorescence-based detection or through localized surface plasmon resonance-based label-free detection. Here, we demonstrate that aerosol-assisted atmospheric plasma deposition could be used to incorporate metal nanostructures in cellulose paper sensors using a completely dry process. Figures 6a and 6b respectively show the XPS data and SEM image of gold nanoparticles on paper. Cellulose paper substrates with and without PEG-like functionalization were coated with gold nanoparticles in order to study the efficacy of the atmospheric-pressure plasma process to incorporate plasmonic nanostructures. Amine-functionalized ssDNA containing Cy3 fluorophore is then dropcast onto both types of substrates with and without gold nanoparticles. The amine functionalities are known to have affinity toward gold nanostructures and the oligos are immobilized on the paper sensors containing gold nanoparticles. Fluorescence measurement in Figure 7 shows

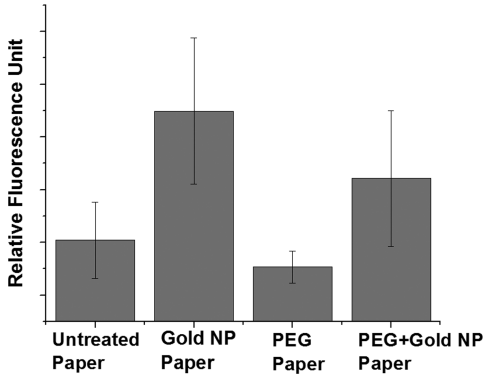

Figure 7. Fluorescence intensity of the untreated and plasma-coated paper sensors dropcast with amine-functionalized ssDNA containing Cy-3 fluorophore.

that the fluorescence intensity is higher in the case of samples containing gold nanoparticles. It is evident, from Figure 6b, that the density of gold nanoparticles on the paper sensors is low. Unlike the amine functionalization, the density of packing of nanomaterials is dependent on several factors, including deposition time, plasma process parameters, distance between the electrode and the substrate, and, more importantly, the concentration of the nanomaterials in the colloidal solution. It is essential to have a high concentration of the nanomaterials in the colloid in order to get a high density of packing. The large

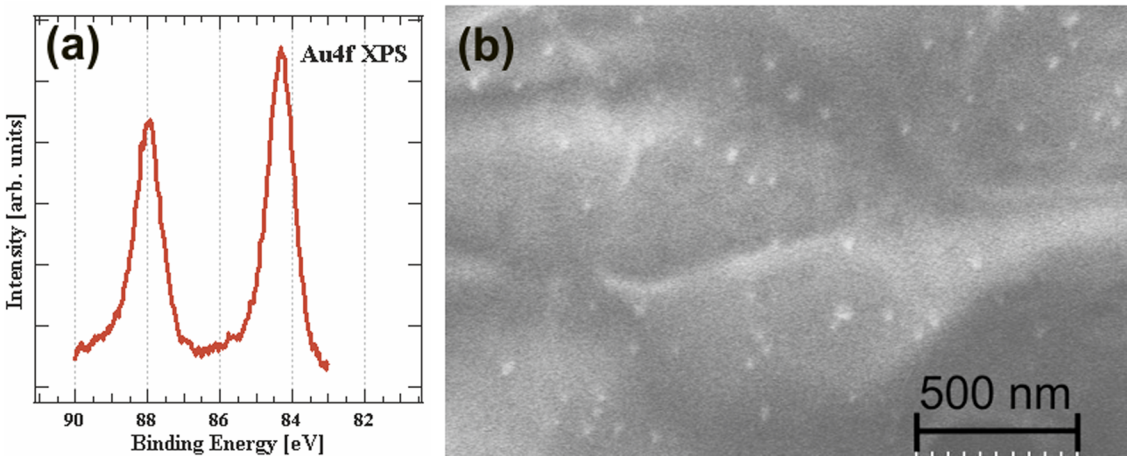

Figure 6. (a) Au 4f core-level photo electron spectroscopy. (b) SEM image of paper containing gold nanoparticles deposited via an atmospheric-pressure plasma process.

error bar in Figure 7 is likely due to the low density of gold nanoparticles on the cellulose.

The ability to create hydrophilic and hydrophobic regions on paper, combined with site-selective surface functionalization and incorporation of plasmonic nanostructures demonstrated here, opens up a range of capabilities and applications in biomedical diagnostics. Further functionalization strategies, such as those of carboxylic, fluorinated, aldehyde, etc., could be adopted, depending on the type of primary antibody or the probe for capturing the ligand in the bioassay. The deposition system presented here could be modified for depositing multiple materials, either simultaneously or sequentially using multiple jets. Each capillary could be connected to either a reservoir containing single precursor material or to multiple reservoirs containing different precursor materials to facilitate multiple depositions. The multijet plasma system can be automated and controlled individually to precisely control the surface characteristics. We have shown that the high-speed, room-temperature, stable, reliable, and solventless plasma polymerization process can help to develop low-cost and highly sensitive biosensor platforms with the potential to replace the wet-chemistry-prepared coatings currently used.

CONCLUSION

Efficient incorporation of bioreactive and biofouling organic functionalities and metal nanostructures for signal amplification in the cellulose fiber network has been demonstrated for the low-cost fabrication of paper sensors. Fluorescence detection of DNA hybdridization on plasma-processed aminated paper, significant reduction of nonspecific binding on PEG functionalized paper, and incorporation of plasmonic nanostructures demonstrated here show the applicability of the paper sensors for DNA detection. A thorough characterization of the surfaces using FTIR, XPS, and NEXAFS provided details about the chemical environment of the functionalized cellulose. Unlike the amino silane precursor, the presence of significant amount of sp_2 hybridized carbon and nitrogen, in addition to sp_3 hybridized amine, demonstrates the extent to which dehydrogenation and formation of multiple bonds could be caused by the fragmentation and cross-linking in the plasma-polymerized film. Although the results presented in this work demonstrate an efficient, reliable, and reproducible fabrication of disposable paper sensor chips, further research is needed to address several interesting questions on plasma diagnostics and electrical characteristics of the aerosol-assisted plasma setup. Since the emerging industry focus is on the efficient fabrication of single-use chips that do not require manipulation of solutions, we believe that the present approach lends itself to rapid, cost-effective, and high-volume manufacturing of biosensor chips in a single process.

ASSOCIATED CONTENT

Supporting Information

Details on the literature assignment of C 1s and N 1s Rydberg transitions in gas and solid phase organics. This material is available free of charge via the Internet at http://pubs.acs.org.

AUTHOR INFORMATION

Corresponding Author

*Tel.: 650 604-2616. Fax: 650 604 5244. E-mail: m.meyyappan@nasa.gov.

Notes

The authors declare no competing financial interest.

ACKNOWLEDGMENTS

This work was supported by the Nanotechnology Thematic Project in NASA's Game Changing Development Program. J.K. acknowledges a Presidential Early Career Award. R.P.G. is with the Universities Space Research Association, subcontracted to NASA Ames Research Center, under a NASA cooperative agreement. Use of the Stanford Synchrotron Radiation Lightsource, SLAC National Accelerator Laboratory, is supported by the U.S. Department of Energy, Office of Science, Office of Basic Energy Sciences under Contract No. DE-AC02-76SF00515. The SSRL Structural Molecular Biology Program is supported by the DOE Office of Biological and Environmental Research, and by the National Institutes of Health, National Institute of General Medical Sciences (including No. P41GM103393). The contents of this publication are solely the responsibility of the authors and do not necessarily represent the official views of NIGMS or NIH.

REFERENCES

(1) Lankelma, J.; Nie, Z.; Carrilho, E.; Whitesides, G. M. Paper-based Analytical Device for Electrochemical Flow-Injection Analysis of Glucose in Urine. *Anal. Chem.* **2012**, *84*, 4147−4152.

(2) Sassolas, A.; Leca-Bouvier, B. D.; Blum, L. J. DNA Biosensors and Microarrays. *Chem. Rev.* **2008**, *108*, 109−139.

(3) Song, Y.; Gyarmati, P.; Araújo, A. C.; Lundeberg, J.; Brumer, H.; Ståhl, P. L. Visual Detection of DNA on Paper Chips. *Anal. Chem.* **2014**, *86*, 1575−1582.

(4) Scida, K.; Li, B.; Ellington, A. D.; Crooks, R. M. DNA Detection Using Origami Paper Analytical Devices. *Anal. Chem.* **2013**, *85*, 9713−9720.

(5) Araujo, A. C.; Song, Y.; Lundeberg, J.; Stahl, P. L.; Brumer, H. Activated Paper Surfaces for the Rapid Hybridization of DNA Through Capillary Transport. *Anal. Chem.* **2012**, *84*, 3311−3317.

(6) Yu, A.; Shang, J.; Cheng, F.; Paik, B. A.; Kaplan, J. M.; Andrade, R. B.; Ratner, D. M. Biofunctional Paper via the Covalent Modification of Cellulose. *Langmuir* **2012**, *28*, 11265−11273.

(7) Su, S. X.; Nutiu, R.; Filipe, C. D. M.; Li, Y. F.; Pelton, R. Adsorption and Covalent Coupling of ATP-binding DNA Aptamers onto Cellulose. *Langmuir* **2007**, *23*, 1300−1302.

(8) Sharma, P.; Basir, S. F.; Nahar, P. Photoimmobilization of Unmodified Carbohydrates on Activated Surface. *J. Colloid Interface Sci.* **2010**, *342*, 202−204.

(9) Aied, A.; Zheng, Yu.; Pandit, A.; Wang, W. DNA Immobilization and Detection on Cellulose Paper using a Surface Grown Cationic Polymer via ATRP. *ACS Appl. Mater. Interfaces* **2012**, *4*, 826−831.

(10) Aied, A.; Glynn, B.; Cao, H.; Zheng, Yu.; Tai, H.; Pandit, A.; Wang, W. A Fluorescently Labeled, Hyperbranched Polymer Synthesized from DE-ATRP for the Detection of DNA Hybridization. *Polym. Chem.* **2012**, *3*, 332−334.

(11) Ademovic, Z.; Wei, J.; Winther-Jensen, B.; Hou, X.; Kingshott, P. Surface Modification of PET Films Using Pulsed AC Plasma Polymerisation Aimed at Preventing Protein Adsorption. *Plasma Process Polym.* **2005**, *2*, 53−63.

(12) Gandhiraman, R. P.; Volcke, C.; Gubala, V.; Doyle, C.; Basabe-Desmonts, L.; Dotzler, C.; Toney, M. F.; Iacono, M.; Nooney, R. I.; Daniels, S.; James, B.; Williams, D. E. High Efficiency Amine Functionalization of Cycloolefin Polymer Surfaces for Biodiagnostics. *J. Mater. Chem.* **2010**, *20*, 4116−4127.

(13) Lin, P. A.; Sankaran, R. M. Plasma-Assisted Dissociation of Organometallic Vapors for Continuous, Gas-Phase Preparation of Multimetallic Nanoparticles. *Angew. Chem., Int. Ed.* **2011**, *50*, 10953−10956.

(14) Tian, L.; Morrissey, J. J.; Kattumenu, R.; Gandra, N.; Kharasch, E. D.; Singamaneni, S. Bioplasmonic Paper as a Platform for Detection of Kidney Cancer Biomarkers. *Anal. Chem.* **2012**, *84*, 9928−9934.
(15) Lee, C. H.; Hankus, M. E.; Tian, L.; Pellegrino, P. M.; Singamaneni, S. Highly Sensitive Surface Enhanced Raman Scattering Substrates Based on Filter Paper Loaded with Plasmonic Nanostructures. *Anal. Chem.* **2011**, *83*, 8953−8958.
(16) Lakowicz, J. R. Plasmonics in Biology and Plasmon-Controlled Fluorescence. *Plasmonics* **2006**, *1*, 5−33.
(17) Connor, N. O.; Gandhiraman, R. P.; Doyle, C.; James, B.; MacCraith, B. D.; Williams, D. E.; Daniels, S. Room Temperature Deposition of Tunable Plasmonic Nanostructures by Atmospheric Pressure Jet Plasma. *J. Mater. Chem.* **2012**, *22*, 9485−9489.
(18) Carrilho, E.; Martinez, A. W.; Whitesides, G. M. Understanding Wax Printing: A Simple Micropatterning Process for Paper-Based Microfluidics. *Anal. Chem.* **2009**, *81*, 7091−7095.
(19) Renault, C.; Li, X.; Fosdick, S. E.; Crooks, R. M. Hollow-Channel Paper Analytical Devices. *Anal. Chem.* **2013**, *85*, 7976−7979.
(20) Tirsell, K. G.; Karpenko, V. P. A General Purpose Sub-keV X-ray Facility at the Stanford Synchrotron Radiation Laboratory. *Nucl. Instrum. Methods Phys. Res., Sect. A* **1990**, *291*, 511−517.
(21) Moravej, M.; Yang, X.; Nowling, G. R.; Chang, J. P.; Hicks, R. F.; Babayan, S. E. Physics of High-Pressure Helium and Argon Radio-Frequency Plasmas. *J. Appl. Phys.* **2004**, *96*, 7011−7017.
(22) Klages, C. P.; Grishin, A. Plasma Amination of Low-Density Polyethylene by DBD Afterglows at Atmospheric Pressure. *Plasma Process Polym.* **2008**, *5*, 368−376.
(23) Petersen, J.; Fouquet, T.; Michel, M.; Toniazzo, V.; Dinia, A.; Ruch, D.; Bomfim, J. A. S. Enhanced Adhesion over Aluminum Solid Substrates by Controlled Atmospheric Plasma Deposition of Amine-Rich Primers. *ACS Appl. Mater. Interfaces* **2012**, *4*, 1072−1079.
(24) Gandhiraman, R. P.; Le, N. C. H.; Doyle, C.; Volcke, C.; Gubala, V.; Uppal, S.; Dixit, C. K.; Monaghan, R.; James, B.; Kennedy, R. O.; Daniels, S.; Williams, D. E. Multi-layered Plasma Polymerized Coatings for SPR Based Biomolecular Detection. *ACS Appl. Mater. Interfaces* **2011**, *3*, 4640−4648.
(25) Coyle, C.; Gandiraman, R. P.; Gubala, V.; Le, N. C. H.; Charlton, C.; Swift, P.; Daniels, S.; Williams, D. E. Tetraethyl Orthosilicate and Acrylic Acid Forming Robust Carboxylic Functionalities on Plastic Surfaces for Biodiagnostics. *Plasma Process Polym.* **2012**, *9*, 28−36.
(26) Raynaud, P.; Despax, B.; Segui, Y.; Caquineau, H. FTIR Plasma Phase Analysis of Hexamethyldisiloxane Discharge in Microwave Multipolar Plasma at Different Electrical Powers. *Plasma Process Polym.* **2005**, *2*, 45−52.
(27) Bierbaum, K.; Kinzler, M.; Woll, Ch.; Grunze, M.; Hahner, G.; Heid, S.; Effenberger, F. A Near Edge X-ray Absorption Fine Structure Spectroscopy and X-ray Photoelectron Spectroscopy Study of the Film Properties of Self-Assembled Monolayers of Organosilanes on Oxidized Si(100). *Langmuir* **1995**, *11*, 512−518.
(28) Smith, B. *Infrared Spectral Interpretation: A Systematic Approach*; CRC Press: Boca Raton, FL, 1998.
(29) White, L. D.; Tripp, C. P. Reaction of (3-Aminopropyl)-dimethylethoxysilane with Amine Catalysts on Silica Surfaces. *J. Colloid Interface Sci.* **2000**, *232*, 400−407.
(30) Theil, J. A.; Tsu, D. V.; Watkins, M.W.; Kim, S. S.; Lucovsky, G. Local Bonding Environments of Si−OH Groups in SiO_2 Deposited by Remote Plasma Enhanced Chemical Vapor Deposition and Incorporated by Postdeposition Exposure to Water Vapor. *J. Vac. Sci. Technol., A* **1990**, *8*, 1374−1381.
(31) Kurth, D. G.; Thomas, B. Thin Films of (3-Aminopropyl)-triethoxysilane on Aluminum Oxide and Gold Substrates. *Langmuir* **1906**, *11*, 3061−3067.
(32) Socrates, G. *Infrared and Raman Characteristic Group Frequencies*; Wiley: Chichester, U.K., 2004.
(33) Van Os, M. T.; Menges, B.; Foerch, R.; Vancso, G. J.; Knoll, W. Characterisation of Plasma Polymerised Allylamine using Optical Waveguide Mode Spectroscopy. *Chem. Mater.* **1999**, *11*, 3252−3257.
(34) Dennis, R. V.; Schultz, B. J.; Jaye, C.; Wang, X.; Fischer, D. A.; Cartwright, A. N.; Banerjee, S. Near Edge A-ray Absorption Fine Structure Spectroscopy Study of Nitrogen Incorporation in Chemically Reduced Graphene Oxide. *J. Vac. Sci. Technol. B* **2013**, *31*, 041204.
(35) Lee, W. H.; Lee, J. G.; Reucroft, P. J. XPS Study of Carbon Fiber Surfaces Treated by Thermal Oxidation in a Gas Mixture of O_2/(O_2+N_2). *Appl. Surf. Sci.* **2001**, *171*, 136−142.
(36) Gubala, V.; Gandhiraman, R. P.; Volcke, C.; Doyle, C.; Coyle, C.; James, B.; Daniels, S.; Williams, D. E. Functionalization of Cycloolefin Polymer Surfaces by Plasma Enhanced Chemical Vapour Deposition: Comprehensive Characterization and Analysis of the Contact Surface and the Bulk of Aminosiloxane Coatings. *Analyst* **2010**, *135*, 1375−1381.
(37) Stohr, J. *NEXAFS Spectroscopy*; Springer: Berlin, 1992.
(38) Groot, F. D.; Kotani, A. *Core Level Spectroscopy of Solids*; CRC Press: Boca Raton, FL, 2008.
(39) Urquhart, S.; Hitchcock, A. P.; Priester, R. D.; Rightor, E. G. Analysis of Polyurethanes Using Core Excitation Spectroscopy. Part II: Inner Shell Spectra of Ether, Urea and Carbamate Model Compounds. *J. Polym. Sci., Part B: Polym. Phys.* **1995**, *33*, 1603−1620.
(40) Ishii, I.; Hitchcock, A. P. The Oscillator Strengths for C 1s and O 1s Excitation of Some Saturated and Unsaturated Organic Acids, Alcohols and Esters. *J. Electron Spectrosc. Relat. Phenom.* **1988**, *46*, 55−64.
(41) Outka, D. A.; Stohr, J.; Madix, R. J.; Rotermund, H. H.; Hermsmeier, B.; Solomon, J. NEXAFS Studies of Complex Alcohols and Carboxylic Acids on the Si(111) (7 × 7) Surface. *Surf. Sci.* **1987**, *185*, 53−74.
(42) Sette, F.; Stöhr, J.; Hitchcock, A. P. Determination of Intra-Molecular Bond Lengths in Gas Phase Molecules from K-Shell Shape Resonances. *J. Chem. Phys.* **1984**, *81*, 4906−4914.
(43) Graf, N.; Yegen, E.; Gross, T.; Lippitz, A.; Weigel, W.; Krakert, S.; Terfort, A.; Unger, W. E. S. XPS and NEXAFS Studies of Aliphatic and Aromatic Amine Species on Functionalized Surfaces. *Surf. Sci.* **2009**, *603*, 2849−2860.
(44) Knorr, D. B.; Jaye, C.; Fischer, D. A.; Shoch, A. B.; Lenhart, J. L. Manipulation of Interfacial Amine Density in Epoxy-Amine Systems as Studied by Near-Edge X-ray Absorption Fine Structure (NEXAFS). *Langmuir* **2012**, *28*, 15294−15304.
(45) Urquhart, S. G.; Ade, H. Trends in the Carbonyl Core (C 1s, O 1s) → π^*C═O Transition in the Near-Edge X-ray Absorption Fine Structure Spectra of Organic Molecules. *J. Phys. Chem. B* **2002**, *106*, 8531−8538.
(46) Solomon, D.; Lehmann, J.; Kinyangi, J.; Liang, B.; Heymann, K.; Dathe, L.; Hanley, K.; Wirick, S.; Jacobsen, C. Carbon (1s) NEXAFS Spectroscopy of Biogeochemically Relevant Reference Organic Compounds. *Soil Sci. Soc. Am. J.* **2009**, *73*, 1817−1830.
(47) Cody, G. D.; Botto, R. E.; Ade, H.; Wirick, S. The Application of Soft X-ray Microscopy to the in-situ Analysis of Sporinite in Coal. *Int. J. Coal Geol.* **1996**, *32*, 69−86.
(48) Cody, G. D.; Ade, H.; Wirick, S.; Mitchell, G. D.; Davis, A. Determination of Chemical Structural Changes in Vitrinite Accompanying Luminescence Alteration using C NEXAFS Analysis. *Org. Geochem.* **1998**, *28*, 441−455.
(49) Kaznacheyev, K.; Osanna, A.; Jacobsen, C.; Plashkevych, O.; Vahtras, O.; Agren, H.; Carravetta, V.; Hitchcock, A. P. Inner-Shell Absorption Spectroscopy of Amino Acids. *J. Phys. Chem. A* **2002**, *106*, 3153−3168.
(50) Stohr, J.; Sette, F.; Johnson, A. L. Near-Edge X-Ray-Absorption Fine-Structure Studies of Chemisorbed Hydrocarbons: Bond Lengths with a Ruler. *Phys. Rev. Lett.* **1984**, *53*, 1684−1687.
(51) Bagus, P. S.; Weiss, K.; Schertel, A.; Wöll, Ch.; Braun, W.; Hellwig, C.; Jung, C. Identification of Transitions into Rydberg States in the X-ray Absorption Spectra of Condensed Long Chain Alkanes. *Chem. Phys. Lett.* **1996**, *248*, 129−135.
(52) Coffey, T.; Urquhart, S. G.; Ade, H. Characterization of the Effects of Soft X-ray Irradiation on Polymers. *J. Electron Spectrosc. Relat. Phenom.* **2002**, *122*, 65−78.

(53) Harder, P.; Bierbaum, K.; Woell, Ch.; Grunze, M.; Heid, S.; Effenberger, F. Induced Orientational Order in Long Alkyl Chain Aminosilane Molecules by Preadsorbed Octadecyltrichlorosilane on Hydroxylated Si(100). *Langmuir* **1997**, *13*, 445−454.
(54) Kallury, K. M. R.; Thompson, M.; Tripp, C. P.; Hair, M. L. Interaction of Silicon Surfaces Silanized with Octadecylchlorosilanes with Octadecanoic Acid and Octadecanamine Studied by Ellipsometry, X-ray Photoelectron Spectroscopy and Reflectance Fourier Transform Infrared Spectroscopy. *Langmuir* **1992**, *8*, 947−954.
(55) Kristensen, E. M. E.; Nederberg, F.; Rensmo, F.; Bowden, T.; Hilborn, J.; Siegbahn, H. Photoelectron Spectroscopy Studies of the Functionalization of a Silicon Surface with a Phosphorylcholine-Terminated Polymer Grafted onto (3-Aminopropyl)trimethoxysilane. *Langmuir* **2006**, *22*, 9651−9657.
(56) Stöhr, J.; Gland, J. L.; Eberhardt, W.; Outka, D.; Madix, R. J.; Sette, F.; Koestner, R. J.; Doebler, U. Bonding and Bond Lengths of Chemisorbed Molecules from Near-Edge X-ray-Absorption Fine-Structure Studies. *Phys. Rev. Lett.* **1983**, *51*, 2414−2417.
(57) Hitchcock, A. P.; Stöhr, J. K-shell Shape Resonances and Intramolecular Bond Length. 'Comments on the Relationship Between Shape Resonances and Bond Lengths. *J. Chem. Phys.* **1987**, *87*, 3523−3525.
(58) Gordon, M. L.; Cooper, G.; Morin, C.; Araki, T.; Turci, C. C.; Kaznatcheev, K.; Hitchcock, A. P. Inner Shell Spectroscopy of the Peptide Bond: Comparison of the C 1s, N 1s and O 1s Spectra of Glycine, Glycyl−Glycine and Glycyl−Glycyl−Glycine. *J. Phys. Chem. A* **2003**, *107*, 6144−6159.
(59) Ishii, I.; Hitchcock, A. P. A Quantitative Experimental Study of the Core Excited Electronic States in Formamide, Formic Acid and Formyl Fluoride. *J. Chem. Phys.* **1987**, *87*, 830−839.
(60) Hitchcock, A. P.; Morin, C.; Tyliszczak, T.; Koprinarov, I. N.; Ikeura-Sekiguchi, H.; Lawrence, J. R.; Leppard, G. G. Soft X-ray Microscopy of Soft Matter—Hard Information From Two Softs. *Surf. Rev. Lett.* **2002**, *9*, 193−201.
(61) Shard, A. G.; Whittle, J. D.; Beck, A. J.; Brookes, P. N.; Bullett, N. A.; Talib, R. A.; Mistry, A.; Barton, D.; McArthur, S. L. A NEXAFS Examination of Unsaturation in Plasma Polymers of Allylamine and Propylamine. *J. Phys. Chem. B* **2004**, *108*, 12472−12480.
(62) Vairavamurthy, A.; Wang, S. Organic Nitrogen in Geomacromolecules: Insights on Speciation and Transformation with K-edge XANES Spectroscopy. *Environ. Sci. Technol.* **2002**, *36*, 3050−3056.
(63) Hitchcock, A. P.; Morin, C.; Heng, Y. M.; Cornelius, R. M.; Brash, J. L. Towards Practical Soft X ray Spectroscopy of Biomaterials. *J. Biomater. Sci., Polym. Ed.* **2002**, *13*, 919−937.
(64) Zhu, Q.; Money, S. L.; Russell, A. E.; Thomas, K. M. Determination of the Fate of Nitrogen Functionality in Carbonaceous Materials during Pyrolysis and Combustion Using X-ray Absorption Near Edge Structure Spectroscopy. *Langmuir* **1997**, *13*, 2149−2157.
(65) Menzies, D. J.; Cowie, B.; Fong, C.; Forsythe, J. S.; Gengenbach, T. R.; McLean, K. M.; Puskar, L.; Textor, M.; Thomsen, L.; Tobin, M.; Muir, B. W. One-Step Method for Generating PEG-like Plasma Polymer Gradients: Chemical Characterization and Analysis of Protein Interactions. *Langmuir* **2010**, *26*, 13987−13994.
(66) Sheth, S. R.; Leckband, D. Measurements of Attractive Forces Between Proteins and End-Grafted Poly(ethylene glycol) Chains. *Proc. Natl. Acad. Sci. U.S.A.* **1997**, *94*, 8399−8404.